St. Louis Area Earthquake Hazards Mapping Project: Seismic and Liquefaction Hazard Maps

by Chris H. Cramer, Robert A. Bauer, Jae-won Chung, J. David Rogers, Larry Pierce, Vicki Voigt, Brad Mitchell, David Gaunt, Robert A. Williams, David Hoffman, Gregory L. Hempen, Phyllis J. Steckel, Oliver S. Boyd, Connor M. Watkins, Kathleen Tucker, and Natasha S. McCallister

ABSTRACT

We present probabilistic and deterministic seismic and liquefaction hazard maps for the densely populated St. Louis metropolitan area that account for the expected effects of surficial geology on earthquake ground shaking. Hazard calculations were based on a map grid of 0.005°, or about every 500 m, and are thus higher in resolution than any earlier studies. To estimate ground motions at the surface of the model (e.g., site amplification), we used a new detailed near-surface shear-wave velocity model in a 1D equivalent-linear response analysis. When compared with the 2014 U.S. Geological Survey (USGS) National Seismic Hazard Model, which uses a uniform firm-rock-site condition, the new probabilistic seismic-hazard estimates document much more variability. Hazard levels for upland sites (consisting of bedrock and weathered bedrock overlain by loess-covered till and drift deposits), show up to twice the ground-motion values for peak ground acceleration (PGA), and similar ground-motion values for 1.0 s spectral acceleration (SA). Probabilistic ground-motion levels for lowland alluvial floodplain sites (generally the 20–40-m-thick modern Mississippi and Missouri River floodplain deposits overlying bedrock) exhibit up to twice the ground-motion levels for PGA, and up to three times the ground-motion levels for 1.0 s SA. Liquefaction probability curves were developed from available standard penetration test data assuming typical lowland and upland water table levels. A simplified liquefaction hazard map was created from the 5%-in-50-year probabilistic ground-shaking model. The liquefaction hazard ranges from low (< 40% of area expected to liquefy) in the uplands to severe (> 60% of area expected to liquefy) in the lowlands. Because many transportation routes, power and gas transmission lines, and population centers exist in or on the highly susceptible lowland alluvium, these areas in the St. Louis region are at significant potential risk from seismically induced liquefaction and associated ground deformation.

INTRODUCTION

St. Louis has experienced minor earthquake damage at least 12 times in the past 205 years. One set of damaging earthquakes for St. Louis was the 1811–1812 New Madrid seismic zone (NMSZ) earthquake sequence. This sequence produced modified Mercalli intensity (MMI) for locations in the St. Louis area that ranged from VI to VIII (Nuttli, 1973; Bakun *et al.*, 2002; Hough and Page, 2011). The region has experienced strong ground shaking (~0.1*g* peak ground acceleration [PGA]) as a result of prehistoric and contemporary seismicity associated with the major neighboring seismic source areas, including the Wabash Valley seismic zone (WVSZ) and NMSZ (Fig. 1), as well as a possible paleoseismic earthquake near Shoal Creek, Illinois, about 30 km east of St. Louis (McNulty and Obermeier, 1997). Another contributing factor to seismic hazard in the St. Louis region is the lower rate of ground-motion attenuation in central and eastern North America compared to western North America (Atkinson, 1984; Campbell, 2003). The consequence is that hazardous ground motions of engineering significance can occur to greater distances in the St. Louis region.

The proximity of the St. Louis region to known active earthquake zones was the motivation for production of digital maps that show the variability of earthquake hazards, including liquefaction and ground shaking, in the St. Louis metropolitan area. These maps estimate how strongly the ground is likely to shake as the result of an earthquake and provide long-term forecasts of earthquake shaking. The maps are more spatially detailed, including local shallow measurements of geologic and geophysical parameters, than the 2014 U.S. Geological Survey (USGS) National Seismic Hazard Maps (NSHM; Petersen *et al.*, 2014), which are based on a generalized firm-rock-site condition.

The St. Louis Area Earthquake Hazards Mapping Project (SLAEHMP) adopts the same earthquake source and earthquake wave propagation models as the 2014 USGS NSHM to address earthquake hazards throughout the study area, a densely populated urban zone, which is split between Missouri and Illinois. The study area is transgressed by the Missouri and Mississippi River floodplains and encompasses about 4000 square kilometers across 29 USGS 7.5 min quadrangles (Figs. 1 and 2). Most of the St. Louis region is underlain by unconsolidated Quaternary deposits that consist of (1) lowlands of alluvium in floodplains along four major rivers (Mississippi, Missouri, Illinois, and Meramec), and (2) uplands of loess over glacial till or drift

 doi: 10.1785/0220160028

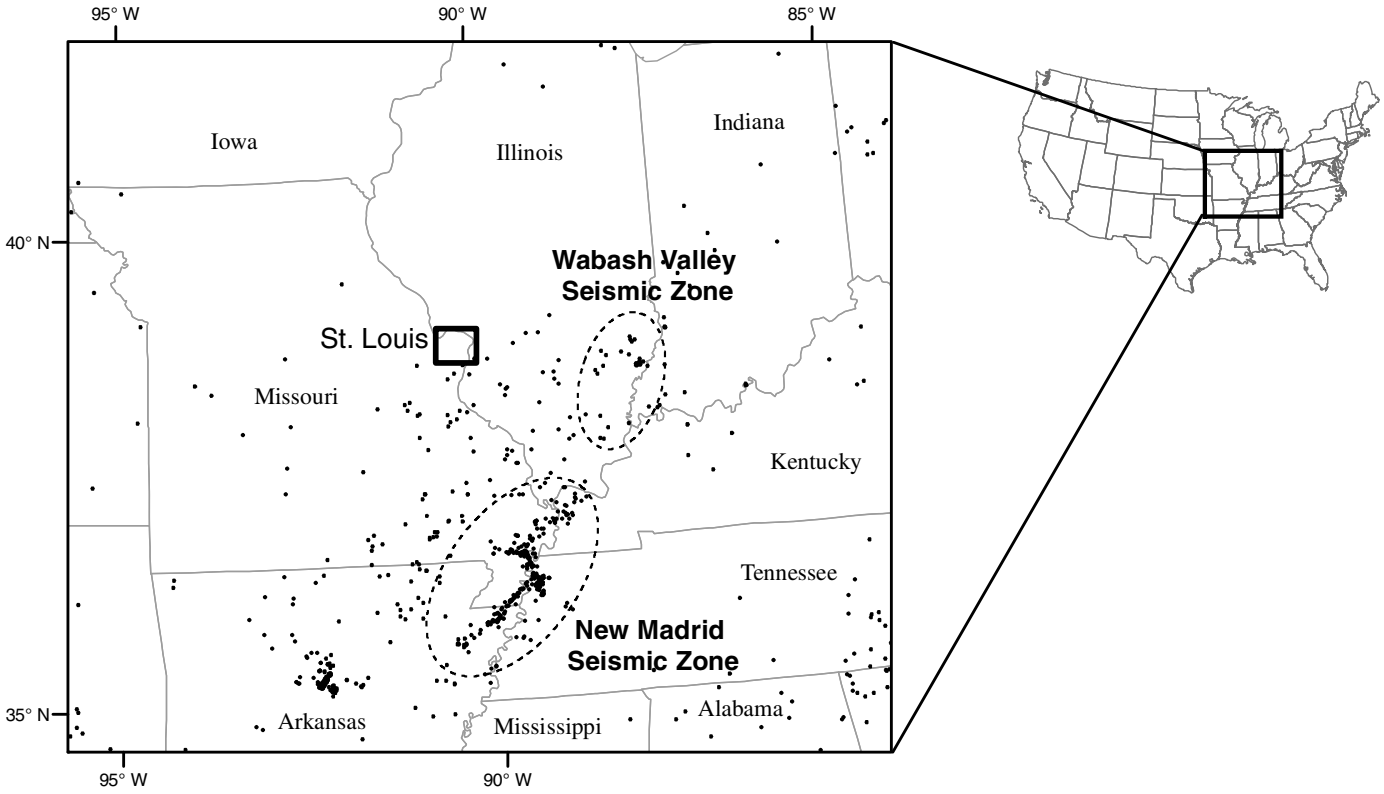

▲ **Figure 1.** Seismicity of the midwestern United States and the areal extent of the New Madrid and Wabash Valley seismic zones relative to the St. Louis area. Dots show earthquakes from 1980 to 2016, **M** 2.5 and larger (up to **M** 5.4; U.S. Geological Survey [USGS] Comcat).

or residuum (Goodfield, 1965; Grimley and Phillips, 2006; Grimley *et al.*, 2007). These thin Quaternary sediments overlie flat-lying sedimentary bedrock, mostly consisting of Mississippian-age limestone and Pennsylvanian-age shale (Harrison, 1997). According to borehole data provided by the Missouri and Illinois Geological Surveys, as well as new geophysical measurements, the depths to bedrock are generally about 30–40 m in the lowlands and about 0–15 m in the uplands.

The St. Louis urban hazard maps are very similar in type and format to the urban hazard maps established by the USGS for the Memphis/Shelby County Seismic Hazard Mapping project completed in 2004 (Cramer *et al.*, 2004, 2006, 2008) and updated in 2013 (Cramer *et al.*, 2014), including the addition of simplified liquefaction hazard for use by nontechnical users. Similar to the Memphis maps, the results are not site specific (results are interpolated and do not include actual geologic and geotechnical information at all map locations; results are approximate). Although the geologic and geophysical model is the most detailed yet produced for the region (based on 7658 geophysical and borehole measurements), it was constructed from nonuniformly spaced data points, and thus the resulting model involves significant interpolation from about 500 m in most areas and up to 5 km in some areas. Further, every location incorporates multiple types of uncertainty, including uncertainty in the depth to bedrock and variability in the shear-wave velocity profile.

Previous efforts to quantify seismic hazards in the St. Louis region include a three quadrangle pilot study and liquefaction susceptibility mapping. In the pilot study, Karadeniz *et al.* (2009) presented a 0.2-s probabilistic hazard map along with a Mississippi River floodplain geologic cross section and a discussion of methodology, geology, and shear-wave velocity. Hoffman (1995), Pearce and Baldwin (2008), and Chung and Rogers (2011) developed liquefaction geology, susceptibility, and potential maps, respectively, for the St. Louis area. This study extends the Karadeniz *et al.* (2009) study area, updates the methodology and data, and provides both scenario and fully probabilistic seismic and liquefaction hazard maps. The methodology used for the probabilistic hazard maps is an updated outside-the-hazard-integral approach for the seismic hazard maps and a recently developed inside-the-hazard-integral approach for liquefaction hazard maps (see Approach section). The data used in the study are improved in resolution and the area covered (see Seismic-Hazard Maps section).

The results of this project are the creation of a database and hazard maps to be used by those in the geosciences, insurance industry, preliminary building design evaluation, and city and county planning agencies to more accurately plan for the adverse effects of earthquakes.

APPROACH

The computer codes used in this study are modified by Cramer (2003, 2014) from the codes used to generate the USGS NSHM.

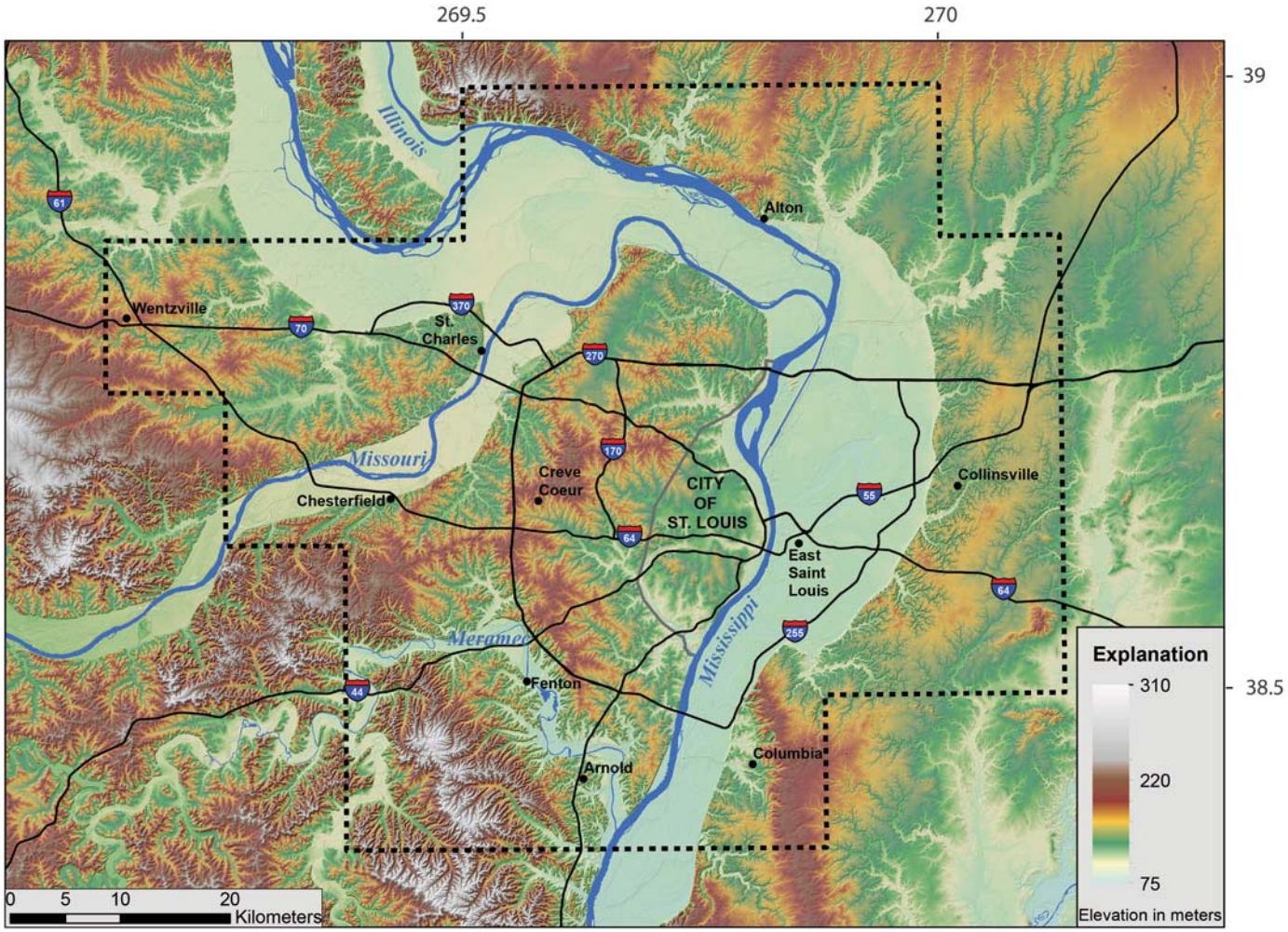

▲ **Figure 2.** For this study, the St. Louis metropolitan area encompasses 29 USGS 7.5 min quadrangles as shown on this shaded relief map. Note the dotted region, which is the 29 quadrangle study area, and the course of the major rivers are included for reference in Figures 6 and 7. Topographic upland areas are readily distinguishable from the modern river lowlands. Major roads are also shown and labeled.

The hazard models and maps developed here use the same set of faults and earthquake sources as in the 2014 NSHM. In developing the probabilistic hazard maps, we use the fully probabilistic approach (Cramer, 2003, 2005) in applying the median and natural logarithm standard deviation of site amplification estimates to hard-rock ground-motion attenuation relations. In the deterministic maps, only the median site amplification is applied. We calculated hazard based on a grid of 0.005°, or about every 500 m, the same spacing employed in calculating the site amplifications. The 500-m grid spacing was selected to provide reasonable resolution near the limit of computational time efficiency (weeks instead of months to produce the site amplification and hazard maps).

Earthquake sources represented in the USGS NSHM and hence in the St. Louis hazard maps are for the NMSZ, the WVSZ, and the distributed seismicity shown in Figure 1. The USGS NSHM also incorporates several additional repeating large magnitude earthquake source zones. These zones include simplifications to earthquake sources developed by the Electric Power Research Institute central and eastern United States–Seismic Source Characterization project (CEUS–SSC, 2012) for the NMSZ and WVSZ, the Commerce geophysical lineament, the Eastern rift margin, and the Marianna paleoseismic site. The distributed or background seismicity is also taken into account in the earthquake source model (see Petersen *et al.*, 2014, for details).

In this study, 1D equivalent-linear soil response analysis was used to evaluate site amplifications and account for soil nonlinearity for the following reasons: (1) high strain levels are not expected; (2) high excess water pressure development is not expected; and (3) the bedrock structure and overlying soft-sediment layering is near horizontal in the St. Louis area. Cramer (2006) demonstrated the appropriateness of using the computationally much more efficient equivalent-linear soil modeling approach instead of nonlinear modeling under these conditions. To account for some of the uncertainty found in St. Louis area shear-wave velocity measurements, shear modulus proxies, depth to bedrock calculations, earthquake time histories, and so on, a Monte Carlo randomization procedure was used to generate site amplification distributions and provide an estimate of the uncertainty, in terms of mean, median, and standard deviation. These distributions were assumed to be lognormal in form.

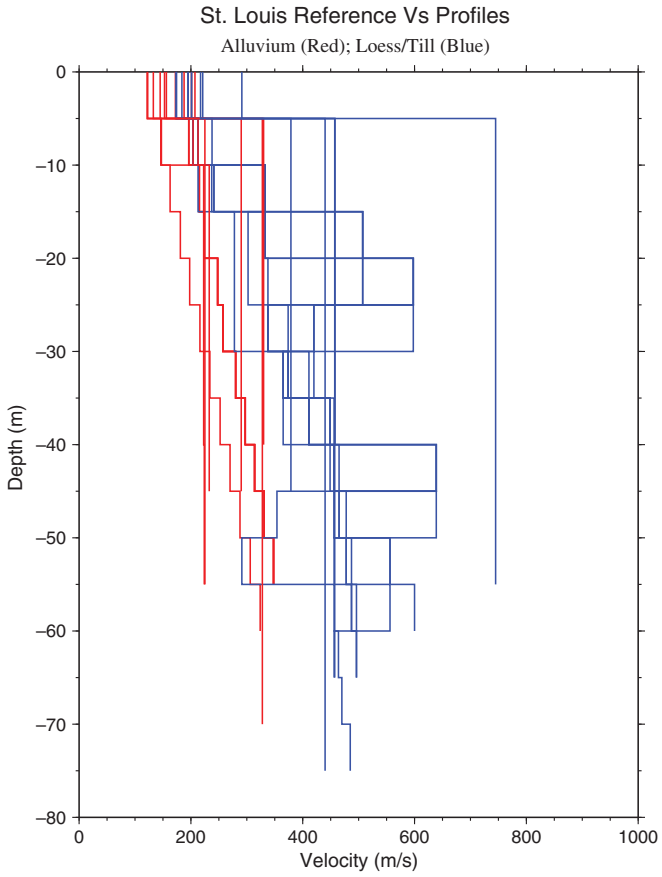

▲ **Figure 3.** Suite of shear-wave velocity (V_S) profiles used in St. Louis area study.

We also generated liquefaction hazard maps for the 29 quadrangles of the study area. Liquefaction probability curves were developed from about 550 geotechnical borings with standard penetration test (SPT) data and lowland and upland water table levels (see LPI Calculation section). These liquefaction probability curves were then used with the probabilistic and scenario ground-shaking hazard maps to calculate liquefaction hazard maps using the approach of Cramer *et al.* (2008). Maps were developed for moderate and severe liquefaction hazard using the probability of the liquefaction potential index (LPI) exceeding 5 and 12, respectively. Simplified shaking and liquefaction hazard have been estimated from the 5%-in-50-year probabilistic hazard maps. The simplified liquefaction hazard map is based on the expected percent area showing liquefaction effects at the surface (probability of LPI exceeding 5).

SEISMIC-HAZARD MAPS

Site Amplification

The method used to calculate site amplification was similar to that employed in the Memphis seismic-hazard maps, summarized in Cramer *et al.* (2004). For each site, time histories for the top of bedrock generated or selected for the St. Louis area (Table 1) were input into the 1D site-response software program SHAKE91 (Idriss and Sun, 1992), which calculates the propagation of the wave through the overlaying soil model (alluvium and loess deposits) above bedrock, producing estimates of the site amplification factors and other parameters. The suite of reference profiles used in this study (keyed to different portions of the study area) is shown in Figure 3 and was developed from over 100 new measurements and 8 compilations of existing data (e.g., Williams *et al.*, 2007; Hoffman *et al.*, 2008).

Anytime we perform a series of calculations that utilizes a series of input variables, uncertainties with each of those variables are compounded, leading to a greater range of uncertainty, bracketing the calculated/reported values. In the assessment of site amplification, uncertainties exist in the following input parameters distinct from measurement uncertainties: (1) shear-wave velocity (e.g., horizontally vs. vertically propagating shear waves, effects of fracture intensity, weathering, and so forth); (2) bulk density (especially with preferential weathering); (3) estimates of the depth and thickness of the soil layers; and (4) the differences in the earthquake time history records used in the 1D shaking analyses. When combined together, these input and measurement uncertainties may cause large differences in calculated amplification. To account for this variability and uncertainty, a random sampling method is usually applied. Cramer *et al.* (2004) used Monte Carlo sampling of estimated amplification parameters to account for the uncertainties associated with the amplification calculations. Cramer (2003) showed that this method is dependable because it accounts for the particular distribution and correlation of uncertainties in the amplification factor.

Site amplifications were calculated for PGA, 0.1, 0.2, 0.3, 0.5, 1.0, and 2.0 s spectral accelerations (SAs). Input site response parameters were randomly selected from a range of shear-wave velocity (V_S) profiles, dynamic soil properties, geologic boundaries, and a suite of earthquake acceleration time histories. SHAKE91 (Idriss and Sun, 1992) was used to calculate the response. The process for selecting input parameters is explained in Cramer *et al.* (2004, 2006).

The amplification distributions were calculated based on a study area grid of about every 500 m. A total of 18,452 grid points encompassed the 29 quadrangles. Figure 4 shows the soil thickness map for the St. Louis area used in this study. For every grid point, the site amplifications and distributions were calculated first, and then the seismic hazard was calculated. The amplification distributions were generated for the appropriate one of 26 distinct geologic units via that unit's geology-based reference V_S profile trimmed to the depth in Figure 4 at a given grid point, and the 500 m grid is thought to be sufficient to capture the differences between these units without imposing months of computational time to produce the hazard maps.

Figure 5 presents example site amplification distributions calculated at a lowlands and an uplands site. Also shown for comparison are the appropriate 2015 National Earthquake Hazards Reduction Program (NEHRP) amplification factors relative to bedrock (class A). Although the NEHRP amplification factors agree fairly well for 1.0 s at the site class D (lowlands) site, they tend to overpredict amplification (near the 84th percentile) relative to the calculated site amplification for 0.2 s at the site class D (lowlands) site and for 1.0 s at the site class C (uplands)

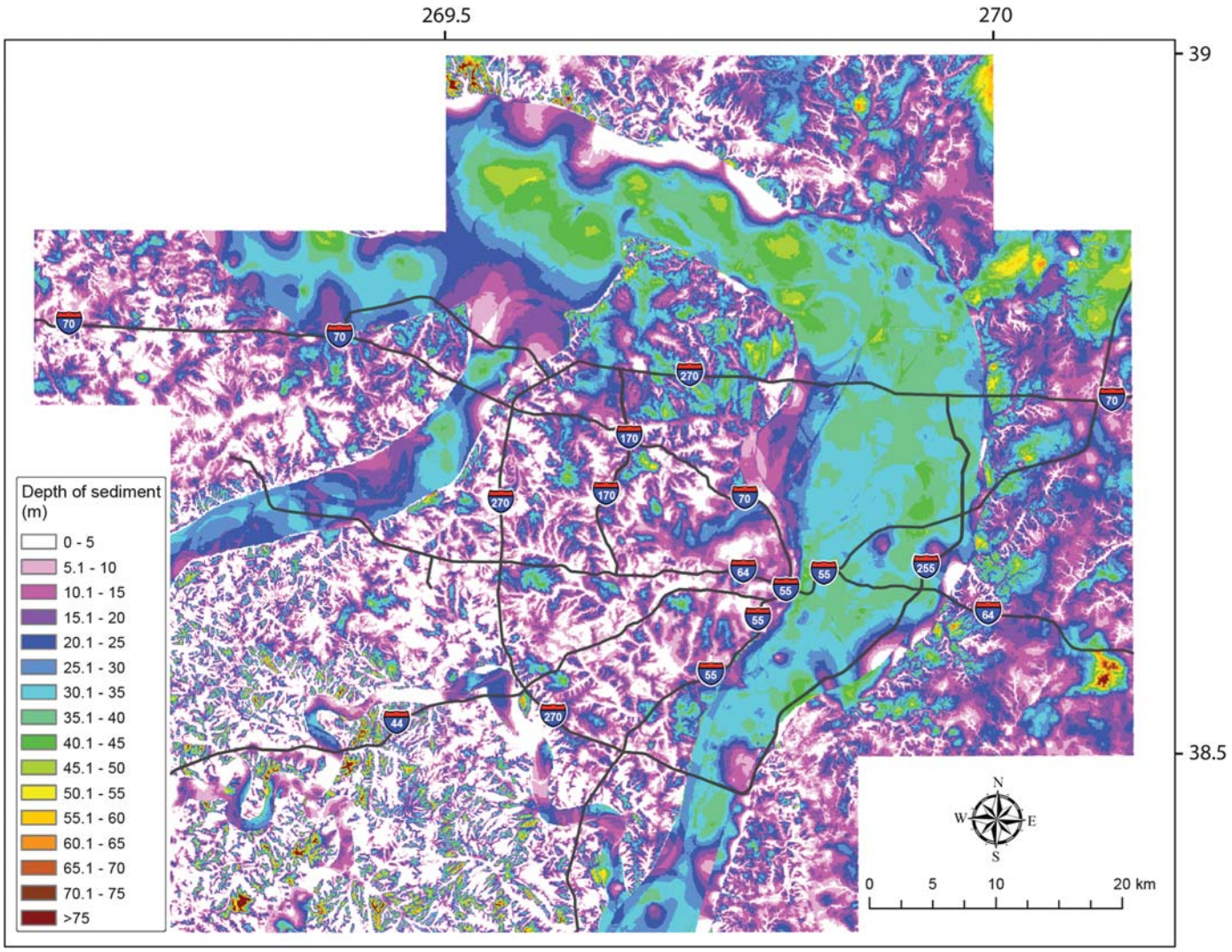

▲ **Figure 4.** Study area sediment thickness map with major highways.

site. The 0.2-s site class C (uplands) NEHRP amplification is relatively flat, whereas the calculated amplification has a strong decreasing amplification with increasing input ground motion due to a greater nonlinear response from local soil profiles that differ significantly from western United States profiles used to develop the NEHRP amplification factors. This demonstrates that the NEHRP amplifications can be too generalized and not specific for central and eastern United States (CEUS) soil profiles. Thus, the calculated amplifications from a CEUS soil profile are more appropriate and better represent CEUS soil response, particularly in a spatially varying soil thickness environment.

Deaggregations showing which earthquake sources contribute to seismic hazard at St. Louis (see Data and Resources) indicate that earthquakes in the **M** 5–6 range predominate within 50 km, and **M** 7s predominate from the 180–200 km distance range; the latter generally representing larger earthquakes originating in the WVSZ and NMSZs (Fig. 1). In this study, the earthquake recordings (time histories) from a database developed for this project were selected to capture the complexity of earthquake time histories at epicentral distances up to 200 km. These recordings are a mix of real earthquake and synthetic earthquake records to better capture natural variability in earthquake ground motions. Separate site amplification distributions were generated for **M** 5, 6, and 7 earthquake sources, with the **M** 5 and 6 amplifications based on records within 50 km and the **M** 7 amplifications based on records in the 150–200-km epicentral distance range. Table 1 presents the selected earthquake recordings used as input at the bottom of the soil column to develop these site amplification distributions at each grid point.

To characterize the ground shaking in a fully probabilistic approach, the areal distribution of site amplification was required. To capture the amplification distributions, the above-mentioned earthquake time histories were scaled up or down to the appropriate ground-motion level. This was accomplished on the actual ground-motion records at 10 different shaking levels (0.01, 0.05, 0.1, 0.2, 0.3, 0.4, 0.5, 0.6, 0.8, and 1.0g) and at specific periods (PGA and 0.1, 0.2, 0.3, 0.5, 1.0, and 2.0 s SA) to obtain the input hard-rock ground motions. We ran the SHAKE91 program for each of these shaking levels and

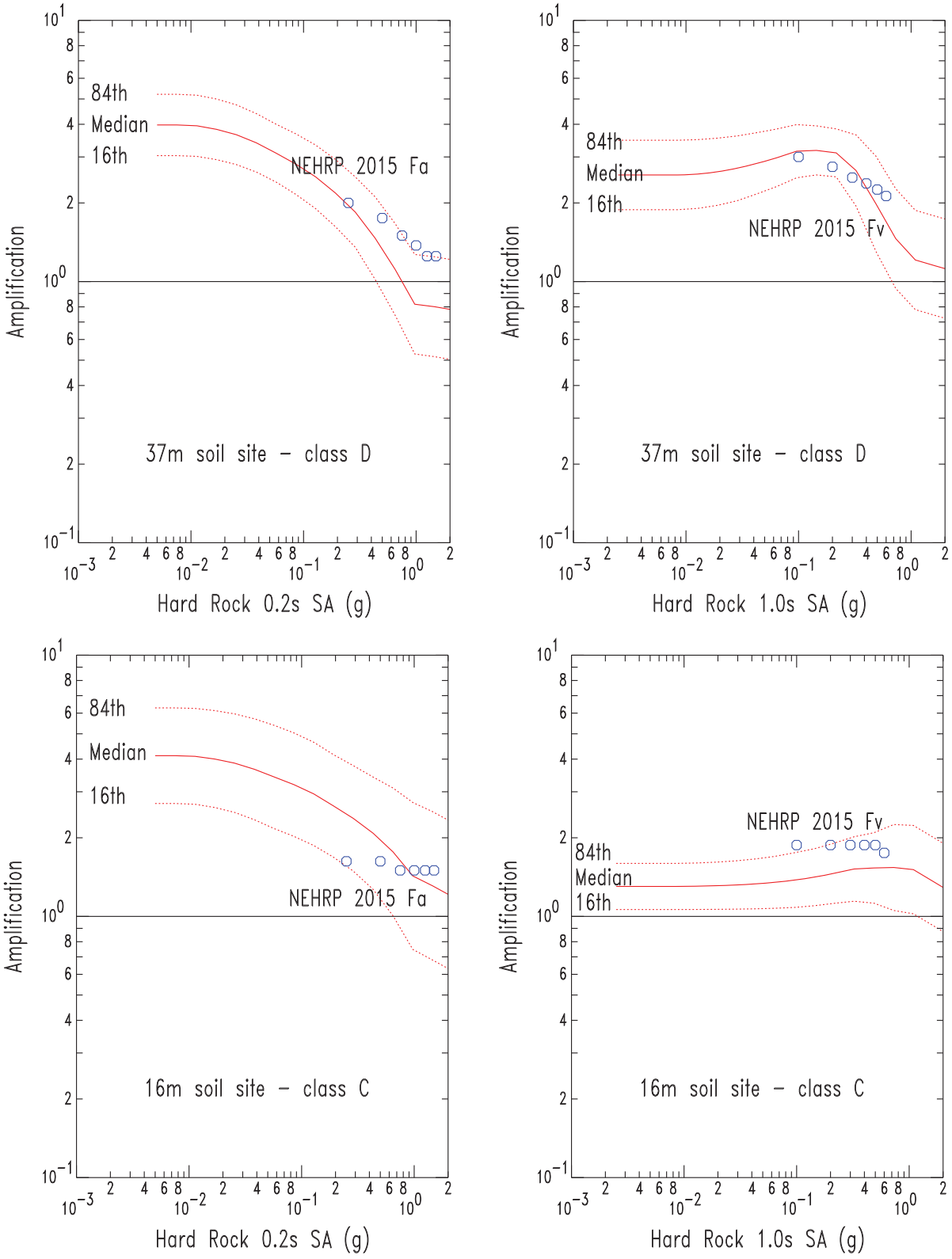

▲ **Figure 5.** Example site amplification distributions for lowlands (top) and uplands (bottom) for 0.2 s (left) and 1.0 s (right) spectral acceleration (SA). Amplifications are relative to bedrock and are shown with the respective 2015 National Earthquake Hazards Reduction Program (NEHRP) Fa and Fv amplification factors (open blue circles) relative to class A (hard rock) for the site class listed in each plot.

Table 1
Suites of Actual and Synthetic M 5, 6, and 7 Earthquake Time Histories Used in the Site Amplification Calculations

Earthquake	Station/Component(s)
***M** 5 Records (19)*	
RiviereDuLoup	CN.A16.HHE, CN.A16.HHN
Saguenay	C016124, C016214
ChiChiAft	TCU071e, TCU071n
CoyoteLake	G01230a, G01320a
FrioliAft	B-SRO000, B-SRO270
LittleSkullMtn	LSM2000, LSM2270
MammothLakesAfter	J-LUL000, J-LUL090
Smsim	m52d030a
Smsim	m55d030a
Smsim	m58d030a
Specmatch	m52d036.olil.e
Specmatch	m52d036.olil.n
***M** 6 Records (15)*	
ChiChiAft	TCU071e, TCU071n
FrioliAft	B-SRO000, B-SRO270
LomaPrieta	G01000,
NorthPalmSprings	WWT180,
Northridge	SAN090, SAN180
Smsim	m62d030a
Smsim	m65d030a
Smsim	m68d030a
Specmatch	m67d047.lit.e
Specmatch	m67d047.lit.s
***M** 7 Records (15)*	
ChiChi	KAU078n, KAU078w
Kobe	TOT000, TOT090
Landers	GRN180, GRN270
Smsim	m72d180a
Smsim	m75d180a
Smsim	m78d180a
AtkBer2002	stlm7p5a
AtkBer2002	stlm8p0a
Specmatch	m69d159.fuk.e
Specmatch	m69d159.fuk.n
Specmatch	m70d195.dcky000.n
Specmatch	m70d195.dcky090.e

Smsim indicates a synthetic time history generated from Stochastic-Method SIMulation (SMSIM; Boore, 1996, 2000), Specmatch indicates a spectrally matched time history using RSPMATCH (N. Abrahamson, written comm., 2005), and AtkBer2002 indicates synthetic time histories using FINSIM by Atkinson and Beresnev (2002) is unnecessary and possibly confusing.

determined the predicted site amplifications for each level. In this study, we used the generic shear modulus and damping ratio relations published by Electric Power Research Institute (1993) corresponding to soil types in the St. Louis area, and we applied an uncertainty of 0.30 natural log units.

Technical Seismic-Hazard Maps

We generated technical seismic-hazard maps using the approach of Cramer *et al.* (2004) with the modifications for magnitude-dependent site amplifications by Cramer (2014). Because of the variation in predominant magnitude with distance cited above, probabilistic hard-rock seismic hazard was calculated for **M** 5s (including down to **M** 4.5), **M** 6s, and **M** 7s separately, and then the appropriate magnitude-dependent site amplification distributions were applied in an outside-the-hazard-integral approach (Lee, 2000; Cramer, 2014). In the outside-the-hazard-integral procedure, site amplifications are assumed to be independent of magnitude and distance so that they can be moved outside the hazard integral and applied to hard-rock hazard curves after the hazard calculation. Finally, the hazard curves from the three magnitude ranges were combined to obtain the total hazard curve for each grid-point specific site in the model. For scenario (deterministic) hazard maps, which are for a specific magnitude earthquake, we used the appropriate **M** 5, 6, or 7 site amplification distributions to convert mean hard-rock scenario hazard to mean geology-specific scenario hazard.

Technical seismic-hazard maps were generated for both probabilistic and scenario cases. The probabilistic maps are for 2%, 5%, and 10% probabilities of exceedance in 50 years. The scenario seismic-hazard maps are for five different earthquake scenarios (not all shown in this article): (1) an **M** 7.5 on the northeast segment of the NMSZ; (2) an **M** 6.0 south of St. Louis near St. Genevieve; (3) an **M** 6.0 east of St. Louis near the Shoal Creek paleoseismic site; (4) an unlikely but plausible **M** 5.8 beneath St. Louis; and (5) an **M** 7.1 near Vincennes, Indiana, in the vicinity of a large paleoseismic earthquake in the WVSZ. Scenario ruptures are between 5 and 60 km in length depending on magnitude. The scenario hazard maps show the median ground-motion hazard for the specified earthquake. We limit our presentation of resulting hazard maps in this article. The 2%-in-50-year probabilistic seismic-hazard maps are shown in Figure 6 for PGA and 1.0 s SA. Figure 7 shows PGA and 1.0 s SA maps for the scenario **M** 5.8 beneath St. Louis, which represents what might be expected from an earthquake similar in magnitude to the 2011 Mineral, Virginia, and 2016 Pawnee, Oklahoma, earthquakes.

SEISMIC-HAZARD DISCUSSION

In Figure 6, the hazard differs from uplands to lowlands and from southeast to northwest. The uplands/lowlands difference is due to thin (< 10 m) versus thicker (30 m or more) soils (see Fig. 4). The southeast to northwest decreasing hazard trend is due to increasing distance from the major earthquake source (NMSZ) by 50 km corresponding to a change in hard-rock PGA of about 0.1*g*. At short periods (PGA), seismic hazard is higher on the bluffs (uplands), mostly in the central and eastern parts of the study area, and exceeds 0.40*g*, whereas in the lowlands high-frequency shaking hazard is reduced (less

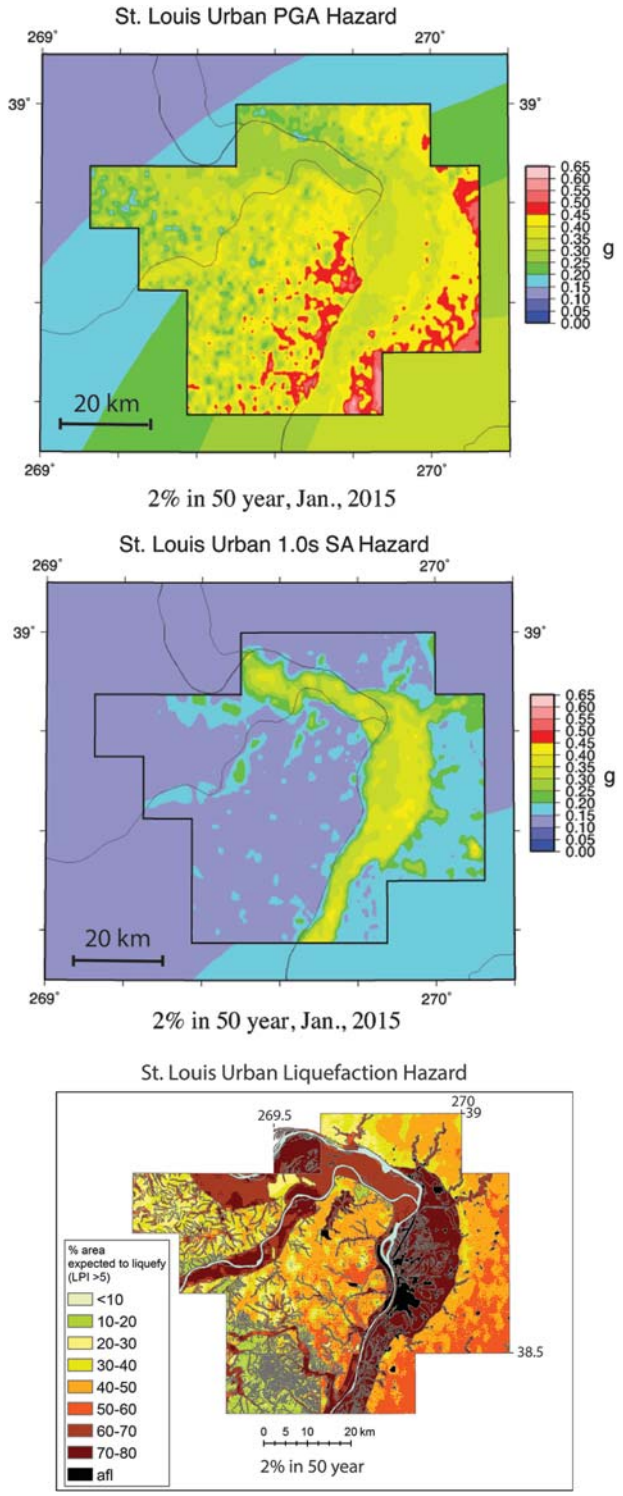

▲ **Figure 6.** St. Louis area urban seismic and liquefaction hazard maps for 2%-in-50-year exceedance values for peak ground acceleration (PGA) (top), 1.0 s SA (middle), and liquefaction potential index greater than 5 (bottom). Urban seismic-hazard maps are inset into the 2014 2%-in-50-year National Seismic Hazard Maps (NSHM) for a firm-rock-site condition (top and middle). January 2015 is the version date of the hazard maps. afl (black) in the liquefaction scale represents artificial fill areas with unknown geotechnical conditions and hence unknown hazard, and are special study zones.

than 0.40*g*, but still capable of causing damage) because of nonlinear soil response damping ground motions. At long periods (1.0 s), the uplands/lowlands trend is reversed with higher seismic hazard (greater than 0.25*g*) in the lowlands, especially along the Mississippi River course, due to soil resonance in thicker soils, whereas being less than 0.25*g* in the uplands (thin soils). These resonances developing in the lowland alluvium overlying bedrock were observed at a Mississippi River floodplain station in St. Louis from an **M** 3.6 earthquake with an epicenter located about 160 km away in southeastern Illinois (Williams *et al.*, 2007).

When compared with the corresponding 2014 NSHMs, the new probabilistic urban seismic-hazard maps show that earthquake ground motions can be up to twice as high as the equivalent NSHM with a firm-rock-site condition (Fig. 6). The short-period (PGA) seismic hazard is higher than the NSHM hazard across the entire study area. For longer period hazard (1.0 s), the new maps indicate that the hazard is higher primarily in the Mississippi River lowland area and roughly the same as the NSHM elsewhere.

The **M** 5.8 scenario event in Figure 7 is richer (stronger) in short periods (PGA) than long periods (1.0 s) because of the magnitude and shallow depth (5 km) of the scenario earthquake. The scenario PGAs range from 0.03*g* to 1.21*g*, whereas the scenario 1.0-s SA values range from 0.01*g* to 0.44*g*. The short-period hazard (PGA) is more relevant to short structures (1–3 stories), and the long-period hazard (1.0 s SA) is more relevant to taller and larger structures (around 10 stories or taller). These scenario 1.0-s SA hazard values can also be used to estimate MMI using the relations of Ogweno and Cramer (2016). For this scenario, it results in MMI VI at the edge of the uplands near the Mississippi River on the east side of the city of St Louis, and MMI VII in the lowlands and thicker sediment areas of the Mississippi River floodplain on the east side of the study area.

To provide a perspective on how these scenario ground motions (Fig. 7) relate to observed damaging ground motions, we look to recent earthquakes in Virginia, New Zealand, and California. Significant damage up to intensity VIII (Worden and Wald, 2016) occurred to unreinforced masonry structures (URMs) in central Virginia from the 2011 **M** 5.8 Virginia earthquake. A strong-motion recorder located about 22 km from the Virginia epicenter recorded a PGA of about 0.27*g* (Chapman, 2013). URM damage in downtown Christchurch, New Zealand, from the 2010 M 7.1 Darfield earthquake (epicenter 40 km away) was significant for recorded PGAs of 0.1*g*–0.2*g*, but lower than from the 2011 **M** 6.3 Christchurch aftershock (epicenter 10 km away). For the aftershock, URM damage was severe from recorded PGAs exceeding 0.3*g* (Moon *et al.*, 2014). For engineered structures in downtown Christchurch, only PGAs exceeding 0.3*g* resulted in some significant damage (Fleischman *et al.*, 2014). Possible significant damage to engineered structures begins at about 0.3*g*. The **M** 6.0 Napa, California, earthquake is also a relevant case to compare with the **M** 5.8 St. Louis scenario. This earthquake occurred about 10 km from Napa, generated PGAs exceeding 50%*g* in the city center, and produced MMI VI–VIII, including cracked and

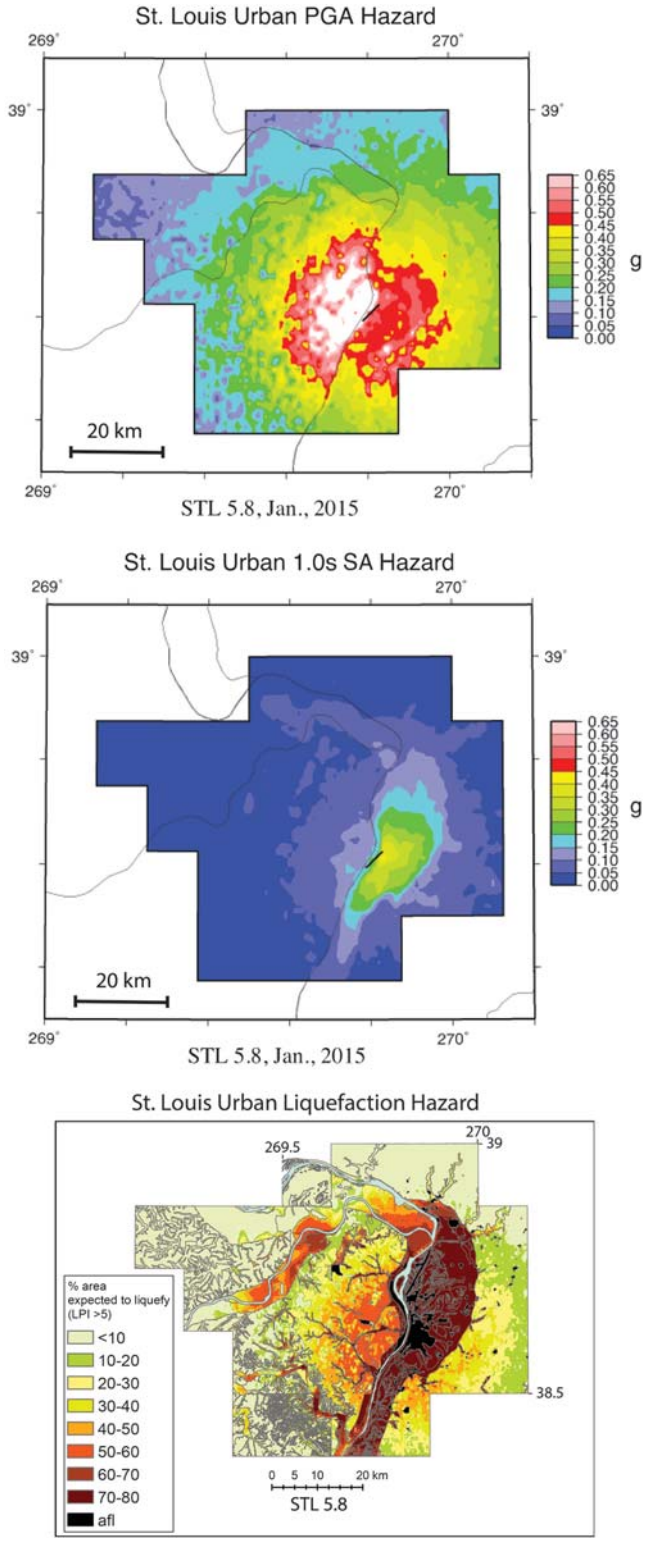

▲ **Figure 7.** St. Louis area urban scenario seismic and liquefaction hazard maps for an unlikely, but plausible, M 5.8 earthquake beneath downtown St. Louis for PGA (top), 1.0 s SA (middle), and liquefaction potential index greater than 5 (bottom). The peak scenario PGA is 1.21*g*. January 2015 is the version date of the hazard maps. afl (black) in the liquefaction scale represents artificial fill areas with unknown geotechnical conditions and hence unknown hazard, and are special study zones.

broken chimneys, broken pipes, and failure of well-built masonry (Baltay and Boatwright, 2015; Boatwright *et al.*, 2015).

LIQUEFACTION HAZARD MAPS

Liquefaction Potential

The LPI (Iwasaki *et al.*, 1978, 1982) has been increasingly applied to evaluate liquefaction hazard worldwide (Holzer *et al.*, 2005; Hayati and Andrus, 2008; Papathanassiou, 2008; Haase *et al.*, 2011). LPI is basically an index of liquefaction potential that integrates the likelihood of liquefaction in a whole soil column and not just a trigger based on a high liquefaction potential at any point in the soil column. Liquefaction potential criteria (zero to minor liquefaction risk when LPI < 5; severe liquefaction risk when LPI > 15) generally correlate well with liquefaction case histories (Iwasaki *et al.*, 1982; Toprak and Holzer, 2003).

Exceeding an LPI value of 15 represents the median value extracted from postearthquake evaluations of liquefied sites over the past half-century (Iwasaki *et al.*, 1978, 1982). Toprak and Holzer (2003) related LPIs with ground damage for the 1989 Loma Prieta earthquake and found that areas with an LPI > 12 were associated with more than 50% of ground cracking (severe hazard) and LPI > 5 for sand boils (moderate hazard). We believe that LPI values of 12 are a conservative estimate of the lower limit of severe liquefaction. Thus, following the procedure of Toprak and Holzer (2003), exceeding LPI values of 12 was adopted as the lower limit of severe liquefaction in this study. Although the use of LPI > 12 for severe liquefaction hazard is more conservative, the impact on the severe liquefaction hazard maps is not so great because areas of severe liquefaction hazard have high probability of severe liquefaction (greater than 60%) using either LPI > 12 or LPI > 15. Highly liquefiable sediments tend to have very high LPIs, which exceed either standard. Additionally, the user community is less interested in severe liquefaction hazard alone and more interested in moderate or greater liquefaction hazard that causes significant enough damage and loss and which is related to LPI > 5.

Cumulative Frequency Distributions

To estimate surface manifestations of liquefaction at a random location within our study area, we followed the approach of Holzer *et al.* (2006), who grouped 202 cone penetration test-based LPI values in surficial geologic units along the margins of San Francisco Bay (140 km^2), California. For St. Louis, we assessed liquefaction hazard based on a model of the physical properties of the unconsolidated surficial deposits and soils developed from analysis of about 550 borehole logs (Chung and Rogers, 2011). The boreholes include data on sample bulk density, SPT-N blow counts, and depth to groundwater. Cumulative frequency distributions of LPI > 5 for surficial geologic units were then analyzed. The percentage of LPI > 5 were interpreted as the probability of surface manifestations of liquefaction.

The LPI method estimates the threshold PGA for specific LPI values and its probability for a scenario earthquake magnitude (e.g., M_w 7.5). Cramer *et al.* (2008) modified the approach to map liquefaction hazards in the Memphis, Tennessee, area using the cumulative frequency distributions for a given LPI

exceedance value. They adjusted the PGA values for various scenario earthquake magnitudes by applying correction factors termed magnitude-scaling factors (MSFs).

Groundwater Depth

The depth of the groundwater table is a controlling factor for assessing liquefaction potential because liquefaction only occurs in saturated soils. High groundwater levels increase the liquefaction potential and increase the LPI values. Liquefaction seldom occurs where the groundwater table is deeper than 12 m below ground surface (Youd, 1973). To demonstrate the effect of water table depth on liquefaction probability, Holzer *et al.* (2011) showed that the liquefaction probabilities decrease significantly when the groundwater table depth increases from 1.5 to 5 m.

Previous probabilistic liquefaction hazard maps (Holzer *et al.*, 2006; Cramer *et al.*, 2008) have been prepared using scenario earthquakes and groundwater levels for an entire study area (e.g., 1.5 m depth for San Francisco Bay; 6 m depth for Memphis). Such blanket assumptions tend to oversimplify liquefaction probability of regional areas. For example, the St. Louis metro area is situated on contrasting geomorphic settings: alluvial floodplains and dissected loess-covered uplands, which exhibit different groundwater depths. The depths to groundwater in the uplands are highly variable, ranging from 1 to 30 m or more (Pearce and Baldwin 2008; Chung and Rogers, 2011, 2012).

To determine the liquefaction probability curves under the most likely conditions, we considered high and normal (similar to low) water table scenarios for both geomorphic provinces (lowlands and uplands), then calculated the liquefaction probabilities for LPI > 5 (moderate) and > 12 (severe liquefaction hazard) at the differing seismic demand of PGA/MSF. Information from the Illinois State Geological Survey (Bauer, 2012) in both the lowlands of the Mississippi floodplain and the uplands provided the estimates for high and normal water table depths used in this study. In the lowlands, water table depths of 0.5 m were used for the high and normal depths. In the uplands, water table depths of 1.0 and 4.0 m were used.

Data

The input data for mapping liquefaction hazard in this study consist of the following components: (1) surficial geologic map, (2) about 550 SPT profiles, and (3) assumed depth-to-groundwater (DTW). The curves of liquefaction probability were established for all assumed water table depths for floodplains and uplands.

LPI Calculation

Following the approach of Romero-Huddock and Rix (2005), who used the simplified SPT-based procedure of Seed and Idriss (1971) and liquefaction resistance curve of Seed *et al.* (1985), we evaluated the critical PGA/MSF sufficient to exceed LPIs of 5 (moderate) and 12 (severe liquefaction effects).

MSF: Among various proposed equations of a MSF, we employed the MSF suggested by Youd *et al.* (2001)

$$\mathrm{MSF} = 10^{2.24}/M_{\mathrm{w}}^{2.56},$$

in which M_{w} is the moment magnitude.

PGA/MSF: Forty-five combinations of PGA ($0.10g$, $0.15g$, $0.20g$, $0.25g$, $0.30g$, $0.35g$, $0.40g$, $0.45g$, and $0.50g$) and M_{w} (6.0, 6.5, 7.0, 7.5, and 8.0) were used to calculate LPI values for each of the surficial geologic units (Fig. 8).

Figure 9 presents the probability of exceeding LPIs of 5 and 12, for high and normal groundwater levels, for the floodplain and upland geomorphic provinces, respectively. The liquefaction probability, as a function of the PGA/MSF, was fitted with a four-parameter Weibull's model, using SigmaPlot software (2006)

$$p = \begin{cases} 1 - e^{-\left(\frac{x - x_0 + b\ln 2^{1/c}}{b}\right)^c} & \text{for } x > x_0 - b\ln 2^{\frac{1}{c}} \\ 0 & \text{for } x \le x_0 - b\ln 2^{\frac{1}{c}} \end{cases}$$

in which $a \times p$ is the liquefaction probability (LPI > 5 or > 12), $x =$ PGA/MSF, a, b, c, and $x_0 =$ fitted coefficients.

The Weibull cumulative probability model is suitable for analyzing the failure probability of composites or layered materials under a given stress (Weibull, 1951; Jibson *et al.*, 2000). This model produces the most versatile sigmoid curve, and is sufficiently flexible to accommodate most data sets. Regression analyses for Weibull's model are presented in Figure 9, and are summarized in Table 2.

Updating Liquefaction Computer Codes

The approach used by Cramer *et al.* (2008) for producing liquefaction hazard maps for Memphis, Tennessee, has been applied to generating liquefaction hazard maps for SLAEHMP. The computer programs used to generate liquefaction hazard maps were updated from the 2002 model to the 2008 model and then to the 2014 USGS national seismic-hazard model-based maps being generated for SLAEHMP. This involved not only updating map generation programs to the 2008 and 2014 hazard model, but also transferring the national map codes to the University of Memphis high-performance computing (HPC) facility. The HPC is needed to calculate both the site amplification distributions and the probabilistic liquefaction hazard in a reasonable amount of time (days instead of months) due to the 0.005° (~500 m) grid used and the number of quadrangles (29) included in the calculations.

The approach of Cramer *et al.* (2008) uses the liquefaction cumulative probability curves of Figure 9. Note that the liquefaction cumulative probability curves are a function of magnitude and hence are used in an inside-the-hazard-integral approach to calculate probabilistic liquefaction hazard maps as indicated in the equation from Cramer *et al.* (2008)

$$P(P_{\mathrm{LPI}>n} > \mathrm{Po}) = \Sigma_i \alpha_i \int_M \int_R f_i(\mathrm{M}) f_i(R) P(P_{\mathrm{LPI}>n} > \mathrm{Po} | A > \mathrm{Ao}, \mathrm{M}) P(A > \mathrm{Ao} | \mathrm{M}, R) dR dM,$$

in which Po is the exceedance probability level, Ao is the exceedance ground motion (PGA) level, $P(P_{\mathrm{LPI}>n} > \mathrm{Po})$ is the liquefaction hazard curve for LPI $> n$, α_i is the rate of source i, M and R are magnitude and distance, $f_i(\mathrm{M})$ and $f_i(R)$ are the ith source magnitude and distance distribution functions, $P(P_{\mathrm{LPI}>n} > \mathrm{Po} | A > \mathrm{Ao}, \mathrm{M})$ is the liquefaction cumulative prob-

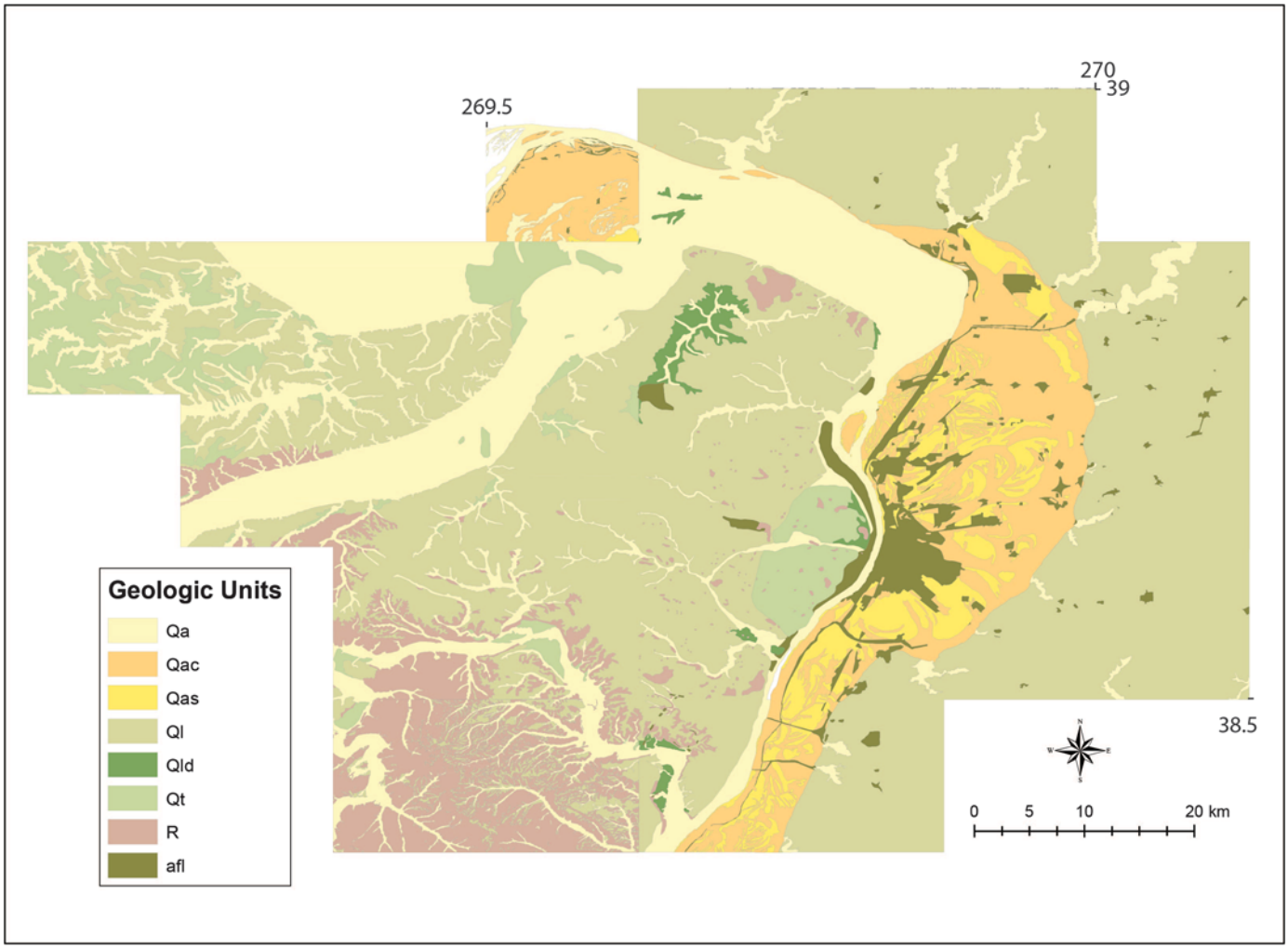

▲ **Figure 8.** Simplified Missouri/Illinois surficial materials map used in liquefaction hazard map generation. Geological unit afl is artificial fill and designates "special study areas" where the geotechnical character of the fill is not known.

ability curve for the site and LPI > n, and $P(A > \text{Ao}|\text{M}, R)$ is the site-specific attenuation relation. The site-specific attenuation relation is generated using the approach of Cramer (2003, 2005).

Liquefaction Hazard Maps

The generation of final liquefaction hazard maps requires the use of a Geographic Information System (GIS), guided by the surface geology map (Fig. 8), to piece together liquefaction hazard maps for each surface soil type into a scenario or probabilistic liquefaction hazard map. With the assistance of Illinois and Missouri geologists, surface geology mapping units were related to the simplified surface geology units used to assign the appropriate liquefaction cumulative probability curves to the detailed surface geology.

We generated scenario liquefaction hazard maps by taking SLAEHMP scenario median PGA hazard maps that include the effects of local geology and applying the median liquefaction cumulative potential curve for the scenario magnitude. At each grid point, the median PGA scaled by the MSF is used to select the probability of exceeding LPI 5 or 12 from the curve for the surface geology at that grid point. SLAEHMP scenario PGA maps are available for: (1) an **M** 7.5 earthquake on the northeast arm of the NMSZ; (2) an **M** 6.0 40 km east of St. Louis near the Shoal Creek, Illinois, paleoliquefaction feature; (3) an **M** 6.0 50 km south-southwest of St. Louis near Sainte Genevieve, Missouri; (4) an M 5.8 beneath downtown St. Louis; and (5) an M 7.1 near Vincennes, Indiana. Only the liquefaction hazard scenario for an **M** 5.8 beneath downtown St. Louis is presented here (Fig. 7).

Once the liquefaction hazard maps for a given scenario or probability of exceedance for each LPI exceedance level, surface geology type, and depth to water table (DTW, high or normal) have been calculated, the two uplands depth to water table alternatives are combined using a weighted average. The SLAEHMP technical working group (TWG) discussed the weighting to be used in combining high and normal water table alternative maps (the two alternatives). After reviewing the water table evidence of Bauer (2012), the TWG weighted the floodplain high DTW map 1.0 and the normal DTW map 0.0, as the reliable evidence in Bauer (2012) showed the floodplain water tables to fluctuate

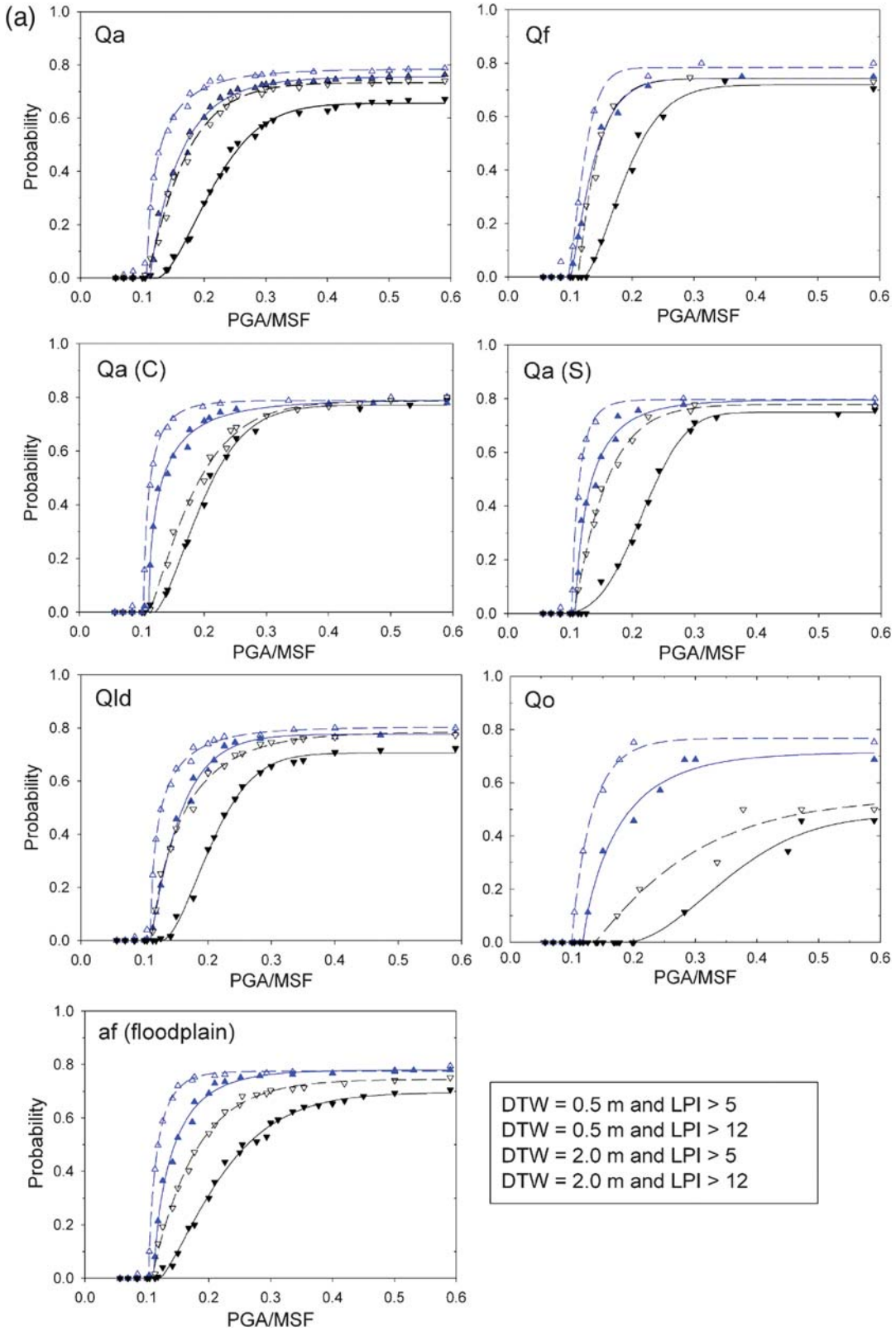

▲ **Figure 9.** (a) Curves of liquefaction probability of liquefaction potential index (LPI) > 5 (open) and LPI > 12 (filled) for surficial geologic units, floodplains within St. Louis area. DTW, depth-to-groundwater (blue, 0.5 m; black, 2.0 m); Qa, alluvium; Qf, alluvial fan; Qa(C), clayey alluvium; Qa(S), sandy alluvium; Qld, lake deposits; Qo, glacial outwash; and af, artificial fills. (b) Curves of liquefaction probability of LPI > 5 (open) and LPI > 12 (filled) for surficial geologic units, uplands within St. Louis area. DTW, depth-to-groundwater (blue, 1.0 m; black, 4.0 m); Ql, loess; Qt, till; R, residuum; and af, artificial fills. (*Continued*)

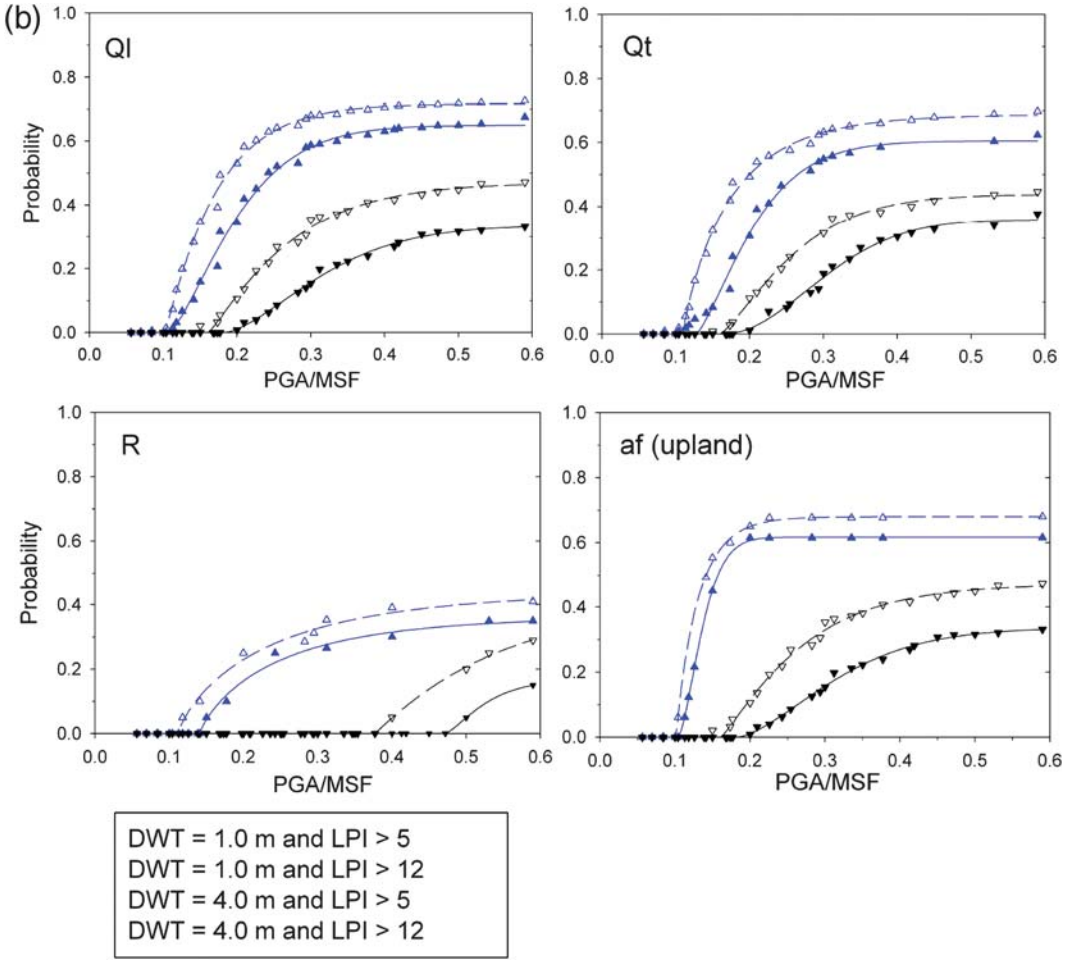

Figure 9. Continued.

between 0.5 and 1.0 m and rarely fall below 1.0 m. For the uplands, the high and normal DTW maps were weighted equally (0.5 each). Thus, for the flood plain surface geology, only the 0.5-m DTW map was used, whereas for the uplands the 1.0 and 4.0 m maps were averaged together.

LIQUEFACTION HAZARD DISCUSSION

Example probabilistic and scenario liquefaction hazard maps are provided for LPI > 5 in Figures 6 and 7 for 2%-in-50-year liquefaction hazard and the **M** 5.8 beneath downtown St. Louis scenario. The related PGA seismic-hazard maps are also shown in those figures. The higher liquefaction susceptible lowland floodplain and old lake-bed soils in the uplands have higher hazard (greater than 60% probability of surface manifestations) than the thin upland soils (less than 60%).

An alternative interpretation of the LPI > 5 liquefaction hazard maps is that they represent the percent area that will liquefy in the indicated surface geology formation during the scenario event or, in the case of the probabilistic maps, with the stated probability of being exceeded. LPI > 5 is the threshold for the onset of liquefaction per our introductory discussion. Areas showing a probability for LPI exceeding 5 of less than 10% have very low likelihood of liquefaction effects at the surface. Probability of LPI > 5 between 10% and 40% should have a low likelihood of liquefaction. For a probability of LPI > 5 between 40% and 60%, the likelihood of liquefaction is moderate. The liquefaction hazard is severe where LPI > 5 exceeding 60% probability.

Using the above criteria, we generated a simplified liquefaction hazard map for very low, low, moderate, and severe liquefaction hazard. We selected the 5%-in-50-year hazard as a good representation of the general hazard level. It represents the shaking hazard from all major earthquakes including the median ground motion from an **M** 7.5 on the northeast arm of the NMSZ (the earthquake with the highest ground motion affecting St. Louis), and hence the liquefaction hazard in the St. Louis area. Figure 10 presents this simplified liquefaction hazard map, which is designed for use by the nontechnical user community to indicate the liquefaction hazard faced in the region. The liquefaction hazard ranges from low in the uplands to severe in the Holocene alluvium of the lowlands, a finding similar to previous studies (e.g., Hoffman, 1995; Pearce and Baldwin, 2008; Chung and Rogers, 2011). Artificial-fill deposits are common in the lowlands and are assigned a "special study required" designation

Table 2
Regression Statistics for Weibull Equation Used in Cumulative Probability Model

Geologic Unit	Groundwater Level	Liquefaction Potential Index (LPI)	Regression Coefficient				R^2
			a	*B*	*c*	X_0	
		Low-Lying Floodplains					
Qa	High	LPI > 5	0.7851	0.0224	0.6093	0.1199	0.9967
		LPI > 12	0.7539	0.0522	0.9356	0.1472	0.9970
	Normal	LPI > 5	0.6366	0.1036	1.3630	0.1940	0.9954
		LPI > 12	0.5702	0.1289	1.2010	0.2494	0.9968
Qa(C)	High	LPI > 5	0.7886	0.0108	0.6288	0.1091	0.9984
		LPI > 12	0.7906	0.0231	0.5745	0.1230	0.9972
	Normal	LPI > 5	0.7744	0.0703	1.2870	0.1632	0.9936
		LPI > 12	0.7693	0.1048	1.1740	0.2255	0.9947
Qa(S)	High	LPI > 5	0.7968	0.0120	0.7968	0.1108	0.9978
		LPI > 12	0.7955	0.0267	0.7067	0.1251	0.9924
	Normal	LPI > 5	0.7829	0.0580	0.8447	0.1759	0.9920
		LPI > 12	0.7729	0.1139	1.2040	0.2474	0.9928
Qf	High	LPI > 5	0.7843	0.0306	1.3580	0.1196	0.9958
		LPI > 12	0.7426	0.0424	1.1970	0.1316	0.9974
	Normal	LPI > 5	0.7389	0.0258	0.9114	0.1553	0.9956
		LPI > 12	0.7158	0.0422	0.6161	0.1967	0.9884
Qld	High	LPI > 5	0.8038	0.0179	0.5673	0.1193	0.9923
		LPI > 12	0.7762	0.0497	1.0670	0.1446	0.9978
	Normal	LPI > 5	0.7022	0.0721	1.2410	0.1971	0.9909
		LPI > 12	0.6652	0.1079	1.1010	0.2670	0.9969
Qo	High	LPI > 5	0.7667	0.0325	0.9235	0.1218	0.9984
		LPI > 12	0.7148	0.0624	0.8399	0.1583	0.9932
	Normal	LPI > 5	0.5463	0.1654	1.0880	0.2544	0.9772
		LPI > 12	0.4778	0.2013	1.8490	0.3507	0.9903
af	High	LPI > 5	0.7752	0.0146	0.7608	0.1120	0.9994
		LPI > 12	0.7802	0.0330	0.7607	0.1313	0.9971
	Normal	LPI > 5	0.6299	0.0989	1.7050	0.1872	0.9939
		LPI > 12	0.6298	0.1335	1.0940	0.2630	0.9979
		Uplands					
Ql	High	LPI > 5	0.7159	0.0718	1.0530	0.1534	0.9976
		LPI > 12	0.6494	0.1076	1.3890	0.1898	0.9964
	Normal	LPI > 5	0.2634	0.1608	0.9990	0.3032	0.9964
		LPI > 12	0.1558	0.2389	2.4300	0.3793	0.9981
Qt	High	LPI > 5	0.6870	0.0668	0.8854	0.1542	0.9975
		LPI > 12	0.6045	0.0911	1.3590	0.1966	0.9930
	Normal	LPI > 5	0.2635	0.2030	0.7729	0.3251	0.9944
		LPI > 12	0.2206	1.2960	0.4311	0.8354	0.9890
af	High	LPI > 5	0.6796	0.0298	0.9545	0.1218	0.9996
		LPI > 12	0.6170	0.0382	1.5250	0.1341	0.9989
	Normal	LPI > 5	0.6446	0.0671	0.4885	0.2294	0.9926
		LPI > 12	0.5720	0.0513	0.7059	0.3108	0.9989

Qa, alluvium; Qa(C), clayey alluvium; Qa(S), sandy alluvium; Qf, alluvial fan; Qld, lake deposits; Qo, glacial outwash; af, artificial fills; Ql, loess; Qt, till; and *R*, residuum. *a*, *b*, *c*, and x_0 are fitted coefficients and R^2 is the coefficient of determination.
(Continued next page.)

Table 2 (continued)
Regression Statistics for Weibull Equation Used in Cumulative Probability Model

Geologic Unit	Groundwater Level	Liquefaction Potential Index (LPI)	Regression Coefficient				
			a	*B*	*c*	X_0	R^2
R	High	LPI > 5	0.4425	0.1297	0.7950	0.1943	0.9935
		LPI > 12	0.3636	0.1106	0.8186	0.2119	0.9948
	Normal	LPI > 5			NA		
		LPI > 12			NA		

Qa, alluvium; Qa(C), clayey alluvium; Qa(S), sandy alluvium; Qf, alluvial fan; Qld, lake deposits; Qo, glacial outwash; af, artificial fills; Ql, loess; Qt, till; and *R*, residuum. *a*, *b*, *c*, and x_0 are fitted coefficients and R^2 is the coefficient of determination.

because their geotechnical and engineering properties are unknown, thus forecasting their response to seismic shaking is too uncertain. Because many transportation routes, power and gas transmission lines, and population centers exist in or on the highly susceptible Holocene alluvium, these areas in the St. Louis region are at significant potential risk from seismically induced liquefaction-related ground deformation.

The liquefaction hazard maps in Figures 6, 7, and 10 are improvements over the liquefaction hazard maps of Hoffman (1995), Pearce and Baldwin (2008), and Chung and Rogers (2011). Hoffman (1995) based his liquefaction susceptibility map on surface geology and the distribution of susceptible alluvial deposits. Pearce and Baldwin (2008) mapped liquefaction susceptibility in more detail than Hoffman (1995) and

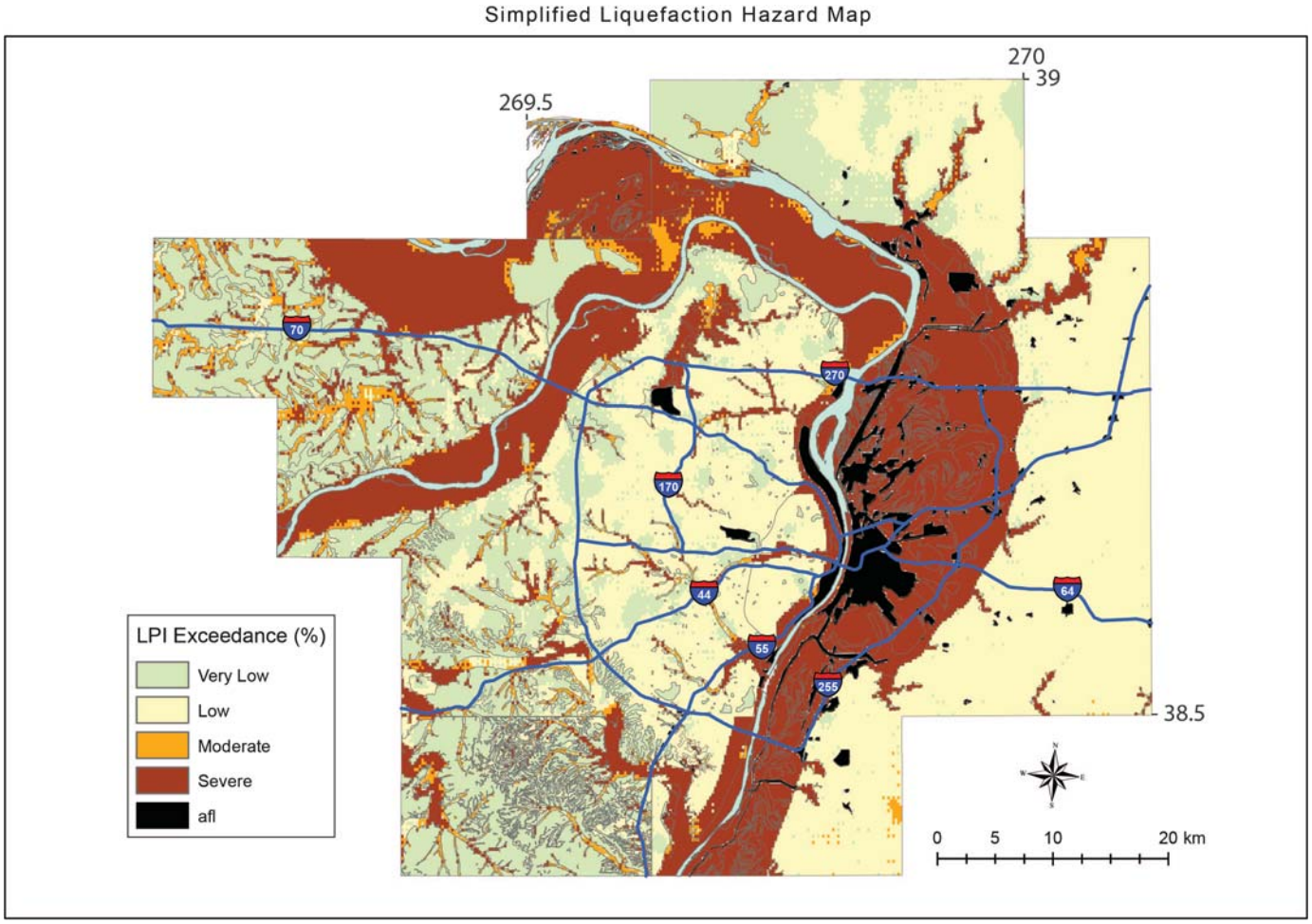

▲ **Figure 10.** Simplified liquefaction hazard map for the St. Louis area. Brown areas have severe liquefaction hazard, orange areas have moderate liquefaction hazard (few occurrences), the light yellow areas have low liquefaction hazard, and light blue areas have very low liquefaction hazard. Black areas are areas of artificial fill with unknown liquefaction potential and hence are "special study" areas requiring further site-specific analysis. Blue lines are major interstate highways.

provided liquefaction susceptibility maps. Chung and Rogers (2011) mapped liquefaction potential using the LPI and generated maps using a constant input ground motion instead of an earthquake scenario ground-motion distribution. The SLAEHMP liquefaction hazard maps are true probabilistic and scenario liquefaction hazard maps incorporating probabilistic and scenario ground-motion distributions with detailed spatial geology and liquefaction probability curves into liquefaction hazard maps, showing what is more likely to occur in a specific earthquake (scenario) or with a given probability of being exceeded (probabilistic).

CONCLUSIONS

The St. Louis metropolitan area, with a population of about 2.8 million, faces earthquake hazard from distant large earthquakes in the NMSZ and WVSZ, as well as a closer region of diffuse historical and prehistoric seismicity to its south and east. Since the moderate MMI VI–VIII damage in the city from the 1811–1812 New Madrid earthquake sequence, these source zones have produced moderate earthquakes that have caused minor damage in the St. Louis area at least 11 times. Also, low attenuation of seismic energy in the region and a substantial number of historic older URM buildings make the St. Louis area vulnerable to moderate earthquakes at relatively large distances compared to the western United States

Using the USGS National Seismic Hazard Model (NSHM) as the foundation, we constructed a new urban seismic-hazard model of the 29 quadrangle study area. We generated both probabilistic and deterministic seismic and liquefaction hazard maps that now include the effects of local geology. The new maps incorporate new surficial geologic mapping and shear-wave velocity measurements, plus a compilation and analysis of about 7500 borings, including about 550 with geotechnical data. These data were the basis for liquefaction analysis, mapping soil thickness and bedrock depth.

Variation in earthquake-shaking hazard in the study area can be subdivided into two main regimes defined by surficial geology: uplands and lowland river valleys, all also uniformly higher than the USGS 2014 NSHM. This is a distinct and important subdivision of seismic hazard that is not contained in the 2014 USGS NSHM for this area. At short periods (PGA), probabilistic seismic hazard is higher on the bluffs (uplands), mostly in the central and eastern parts of the study area, and exceeds 0.40*g*, while in the lowlands high-frequency shaking hazard is reduced (less than 0.40*g*, but still potentially damaging) because of nonlinear soil response damping ground motions. At long periods (1.0 s), the uplands/lowlands trend is reversed with higher seismic hazard (greater than 0.25*g*) in the lowlands, especially along the Mississippi River, due to soil resonance in thicker soils, whereas being less than 0.25*g* in the uplands (thin soils). Liquefaction hazard is characterized as very low (liquefaction unlikely) to severe (liquefaction very likely), with the severe liquefaction hazard occurring in the Mississippi, Missouri, and Meramec River floodplains where there are shallow water tables and 10–40-m-thick sequences of unconsolidated Quaternary sands and gravels over Paleozoic sedimentary rocks.

There are two major caveats associated with the St. Louis area urban hazard maps. The first is that they are regional hazard maps and are not site-specific hazard maps due to the uncertainties associated with the ~500−m grid used in the calculations and the limitations of the geologic model, which required large interpolations between known data points in some cases. Second, these maps, while more accurate than the 2014 USGS NSHM and useful for guidance in developing a site-specific analysis, earthquake-hazard mitigation, preliminary site evaluations, and emergency management decision making, are not yet formally adopted building code maps and have not yet been accepted for the building code regulatory process. We hope the use of these new maps expands across the St. Louis regional planning community. The maps could be improved in the future with better seismic source characterization (recurrence intervals, maximum magnitude) near St Louis and with refinements in ground-motion prediction equations and the physical properties of soils in the alluvial valleys.

DATA AND RESOURCES

SLAEHMP supporting data, geologic maps, and databases are available at http://earthquake.usgs.gov/hazards/urban/st_louis.php (last accessed October 2016). Figures were generated using Generic Mapping Tools (GMT; Wessel and Smith, 1991), Seismic Analysis Code (SAC, Goldstein *et al.*, 2003), and ArcInfo 10.1. Deaggregation website is available at http://geohazards.usgs.gov/deaggint/2008/ (last accessed October 2016).

ACKNOWLEDGMENTS

This research was supported by U.S. Geological Survey (USGS) Earthquake Hazards Program, Department of Interior, under USGS Awards, including GP13AP00030, G11AP20124, G11AP20125, G10AC00224, G09AP00008, and G08HQRG0016. Members of the St. Louis project have worked with local partners to develop detailed maps for urban areas vulnerable to strong ground shaking. In the St. Louis area, these partners include the Center for Earthquake Research and Information (CERI) at the University of Memphis, Missouri University of Science and Technology-Rolla (Missouri S&T), Missouri Department of Natural Resources (MDNR), Illinois State Geological Survey (ISGS), Saint Louis University, Missouri State Emergency Management Agency, and the URS Corporation. The urban hazard maps for the 29 quadrangle St. Louis study area have been produced and evaluated by St. Louis Area Earthquake Hazards Mapping Project (SLAEHMP). The authors gratefully acknowledge reviews by Art Frankel, Chuck Mueller, Jill MCarthy, and an anonymous journal reviewer, which greatly helped to improve the article. Any use of trade, firm, or product names is for descriptive purposes only and does not imply endorsement by the U.S. Government.

REFERENCES

Atkinson, G. (1984). Attenuation of strong ground motion in Canada from a random vibrations approach, *Bull. Seismol. Soc. Am.* **74,** 2629–2653.

Atkinson, G. M., and I. A. Beresnev (2002). Ground motions at Memphis and St. Louis from M 7.5–8.0 earthquakes in the New Madrid seismic zone, *Bull. Seismol. Soc. Am.* **92,** 1015–1024.

Bakun, W. H., A. C. Johnston, and M. G. Hopper (2002). Modified Mercalli intensities (MMI) for large earthquakes near New Madrid, Missouri, in 1811–1812 and near Charleston, South Carolina, in 1886, *U.S. Geol. Surv. Open-File Rept. 02-184*, 32 pp., available at http://pubs.usgs.gov/of/2002/0184/ (last accessed October 2016).

Baltay, A. S., and J. Boatwright (2015). Ground-motion observations of the 2014 South Napa earthquake, *Seismol. Res. Lett.* **86,** 355–360, doi: 10.1785/0220140232.

Bauer, R. A. (2012). Cooperative agreement proposal to the USGS to complete St. Louis area earthquake hazards mapping project's seismic and liquefaction hazard maps: Illinois State Geological Survey depth to groundwater report, *ISGS Final Technical Report*, 15 pp.

Boatwright, J., J. L. Blair, B. T. Aagaard, and K. Wallis (2015). The distribution of red and yellow tags in the City of Napa, *Seismol. Res. Lett.* **86,** 361–368, doi: 10.1785/0220140234.

Boore, D. M. (1996). SMSIM: Fortran programs for simulating ground motions from earthquakes: Version 1.0, *U.S. Geol. Surv. Open-File Rept. 96-80A and 96-80B*, 73 pp.

Boore, D. M. (2000). SMSIM: Fortran programs for simulating ground motions from earthquakes: Version 2.0: A revision of OFR 96-80-A, *U.S. Geol. Surv. Open-File Rept.* 00–509.

Campbell, K. W. (2003). Prediction of strong ground motion using the hybrid empirical method and its use in the development of ground-motion (attenuation) relations in eastern North America, *Bull. Seismol. Soc. Am.* **93,** 1012–1033.

Central and Eastern United States–Seismic Source Characterization (CEUS–SSC) (2012). Central and eastern United States seismic source characterization for nuclear facilities, U.S. Dept. of Energy/Electric Power Research Institute/U.S. Nuclear Regulatory Commission, 3176 pp., www.ceus-ssc.com (last accessed October 2016).

Chapman, M. C. (2013). On the rupture process of the 23 August 2011 Virginia earthquake, *Bull. Seismol. Soc. Am.* **103,** 613–628.

Chung, J.-W., and J. D. Rogers (2011). Simplified method for spatial evaluation of liquefaction potential in the St. Louis area, *J. Geotech. Geoenviron. Eng.* **137,** no. 5, 505–515.

Chung, J.-W., and J. D. Rogers (2012). Interpolations of groundwater table elevation in dissected uplands, *Ground Water* **50,** 598–607, doi: 10.1111/j.1745-6584.2011.00889.x.

Cramer, C. H. (2003). Site-specific seismic-hazard analysis that is completely probabilistic, *Bull. Seismol. Soc. Am.* **93,** no. 4, 1841–1846.

Cramer, C. H. (2005). Erratum to "Site-specific seismic-hazard analysis that is completely probabilistic," *Bull. Seismol. Soc. Am-.* **95,** 2026.

Cramer, C. H. (2006). Quantifying the uncertainty in site amplification modeling and its effects on site-specific seismic-hazard estimation in the upper Mississippi embayment and adjacent regions, *Bull. Seismol. Soc. Am.* **96,** 2008–2020.

Cramer, C. H. (2014). Magnitude dependent site amplification seismic hazard calculation outside the hazard integral for St. Louis, MO (abstract), *Seismol. Res. Lett.* **85,** 542.

Cramer, C. H., J. S. Gomberg, E. S. Schweig, B. A. Waldron, and K. Tucker (2004). The Memphis Shelby County Tennessee seismic hazard maps: *U.S. Geol. Surv. Open-File Rept. 2004–1294*, 41 pp.

Cramer, C. H., J. S. Gomberg, E. S. Schweig, B. A. Waldron, and K. Tucker (2006). First USGS urban seismic hazard maps predict the effects of soils, *Seismol. Res. Lett.* **77,** 23–29.

Cramer, C. H., G. J. Rix, and K. Tucker (2008). Probabilistic liquefaction hazard maps for Memphis, Tennessee, *Seismol. Res. Lett.* **79,** no. 3, 416–423.

Cramer, C. H., R. B. Van Arsdale, M. S. Dhar, D. Pryne, and J. Paul (2014). Updating of urban seismic-hazard maps for Memphis and Shelby County, Tennessee: geology and V_S observations, *Seismol. Res. Lett.* **85,** 986–996.

Electric Power Research Institute (1993). *Guidelines for Determining Design Basis Ground Motions, Palo Alto, California*, Vol. 1/5, EPRI TR-102293, Electric Power Research Institute,.

Fleischman, R. B., J. I. Restrepo, S. Pampanin, J. R. Maffei, K. Seeber, and F. A. Zahn (2014). Damage evaluations of precast concrete structures in the 2010–2011 Canterbury earthquake sequence, *Earthq. Spectra* **30,** no. 1, 272–306.

Goldstein, P., D. Dodge, M. Firpo, and I. Minner (2003). SAC2000: Signal processing and analysis tools for seismologists and engineers, in *Invited contribution to The IASPEI International Handbook of Earthquake and Engineering Seismology*, W. H. K. Lee, H. Kanamori, P. C. Jennings, and C. Kisslinger (Editors), Academic Press, London.

Goodfield, A. G. (1965). Pleistocene and surficial geology of the city of St. Louis and the adjacent St. Louis County, Missouri, *Ph.D. Thesis*, University of Illinois at Urbana-Champaign, 214 pp.

Grimley, D. A., and A. C. Phillips (2006). Surficial geology of Madison County, Illinois: Illinois State Geological Survey, *Illinois Preliminary Geologic Map IPGM Madison County-SG*, scale 1:100, 000, http://www.isgs.illinois/maps/county-maps/surficial-geology/madison (last accessed October 2016).

Grimley, D. A., A. C. Phillips, L. R. Follmer, H. Wang, and R. S. Nelson (2007). Quaternary and environmental geology of the St. Louis metro east area, in *Guidebook for Field Trip for the 35th Annual Meeting of the North-Central Section of the Geological Society of America: Illinois State Geological Survey Guidebook*, David Malone (Editor), Vol. 33, 21–73.

Haase, J. S., Y. S. Choi, R. L. Nowack, C. H. Cramer, O. S. Boyd, and R. A. Bauer (2011). Liquefaction hazard for the region of Evansville, Indiana, *U.S. Geol. Surv. Open-File Rept. 2011–1203*, 38 pp.

Harrison, R. W. (1997). Bedrock geologic map of the St. Louis, $30' \times 60'$ quadrangle, Missouri and Illinois, *U. S. Geol. Surv. Misc. Invest. Ser. Map I-2533*, scale 1:100, 000.

Hayati, H., and R. D. Andrus (2008). Liquefaction potential map of Charleston, South Carolina based on the 1886 earthquake, *J. Geotech. Geoenviron. Eng.* **134,** no. 6, 815–828.

Hoffman, D. (1995). Earthquake hazard map of the St. Louis, Missouri metro area, State of Missouri, Department of Natural Resources, Division of Geology and Land Survey (now Missouri Geological Survey), and State Emergency Management Agency.

Hoffman, D., N. Anderson, and J. D. Rogers (2008). St. Louis, metro area shear wave velocity testing, *U.S. Geol. Surv. Final Tech. Rept.*, available at http://earthquake.usgs.gov/research/external/reports/06HQGR0026.pdf (last accessed February 2016).

Holzer, T. L., M. J. Bennett, T. E. Noce, A. C. Padovani, and J. C. Tinsley (2006). Liquefaction hazard mapping with LPI in the Greater Oakland, California, area, *Earthq. Spectra* **22,** no. 3, 693–708.

Holzer, T. L., T. E. Noce, and M. J. Bennett (2011). Liquefaction probability curves for surficial geologic deposits, *Environ. Eng. Geosci.* **17,** no. 1, 1–21.

Holzer, T. L., T. E. Noce, M. J. Bennett, J. C. Tinsley III, and L. I. Rosenberg (2005). Liquefaction at Oceano, California, during the 2003 San Simeon earthquake, *Bull. Seismol. Soc. Am.* **95,** no. 6, 2396–2411.

Hough, S. E., and M. Page (2011). Toward a consistent model for strain accrual and release for the New Madrid seismic zone, central United States, *J. Geophys. Res.* **116,** no. B3, B03311, doi: 10.1029/2010JB007783.

Idriss, I. M., and J. I. Sun (1992). User's manual for SHAKE91, Center for Geotechnical Modeling, Department of Civil and Environmental Engineering, University of California, Davis, California.

Iwasaki, T., K. Tokida, F. Tatsuoka, S. Watanabe, S. Yasuda, and H. Sato (1982). Microzonation for soil liquefaction potential using simplified methods, *Proc. of 3rd International Conference on microzonation*, Seattle, United States, 28 June– 1 July 1982, 1319–1330.

Iwasaki, T., K. Tokida, F. Tatsuoko, and S. Yasuda (1978). A practical method for assessing soil liquefaction potential based on case studies

at various sites in Japan, *2nd International Conference on Microzonation*, San Francisco, 26 November–1 December 1978, 885–896.
Jibson, R. D., E. L. Harp, and J. A. Michael (2000). A method for producing digital probabilistic seismic landslide hazard maps, *Eng. Geol.* **58,** nos. 3/4, 271–289.
Karadeniz, D., J. D. Rogers, R. A. Williams, C. H. Cramer, R. A. Bauer, D. Hoffman, J. Chung, G. L. Hempen, P. J. Steckel, O. S. Boyd, C. M. Watkins, N. S. McCallister, and E. Schweig (2009). St. Louis Area Earthquake Hazards Mapping Project: A progress Report, November 2008, *U.S. Geol. Surv. Open-File Rept. 2009-1059*, 17 pp.
Lee, R. C. (2000). A methodology to integrate site response into probabilistic seismic hazard analysis, Site Geotechnical Services, Savannah River Site, *Report of 3 February 2000*.
McNulty, W. E., and S. F. Obermeier (1997). Liquefaction evidence for two Holocene paleo-earthquakes in central and southwestern Illinois, *U.S. Geol. Surv. Open-File Rept. 97-435*, 23 pp., available at http://pubs.usgs.gov/of/1997/0435/report.pdf (last accessed October 2016).
Moon, L., D. Dizhur, I. Senaldi, H. Derakhashan, M. Griffith, G. Magenes, and J. Ingham (2014). The demise of the URM building stock in Christchurch during the 2010–2011 Canterbury earthquake sequence, *Earthq. Spectra* **30,** no. 1, 253–276.
Nuttli, O. W. (1973). The Mississippi Valley earthquakes of 1811 and 1812: Intensities, ground motion, and magnitudes, *Bull. Seismol. Soc. Am.* **63,** 227–248.
Ogweno, L. P., and C. H. Cramer (2016). Improved CENA regression relationships between Modified Mercalli Intensities and ground motion parameters, *Bull. Seismol. Soc. Am* **107,** no. 1, doi: 10.1785/0120160033.
Papathanassiou, G. (2008). LPI-based approach for calibrating the severity of liquefaction-induced failures and for assessing the probability of liquefaction surface evidence, *Eng. Geol.* **96,** nos. 1/2, 94–104.
Pearce, J. T., and J. N. Baldwin (2008). Liquefaction susceptibility and probabilistic liquefaction potential hazard mapping, St. Louis, Missouri and Illinois, *National Earthquake Hazards Reduction Program, Final Technical Report*, 51 pp., available at http://earthquake.usgs.gov/research/external/reports/05HQGR0063.pdf (last accessed October 2016).
Petersen, M. D., M. Moschetti, P. Powers, C. Mueller, K. Haller, A. Frankel, Y. Zeng, S. Rezaeian, S. Harmsen, O. Boyd, N. Field, R. Chen, K. Rukstales, N. Luco, R. Wheeler, R. Williams, and A. Olsen (2014). The 2014 update of the United States national seismic hazard models, *U.S. Geol. Surv. Open-File Rept. 2014-1091*, 255 pp., available at http://pubs.usgs.gov/of/2014/1091/ (last accessed October 2016).
Romero-Huddock, S., and G. J. Rix (2005). Liquefaction potential mapping in Memphis/Shelby County, Tennessee, in *Seminar on New Knowledge of Earthquake Hazard in the Central United States and Implications for Building Seismic Design Practice, March 3, 2005, Memphis, Tennessee Speaker Handouts, 7-15-7-32*, Redwood City, California, Applied Technology Council.
Seed, H. B., and I. M. ldriss (1971). Simplified procedure for evaluating soil liquefaction potential, *J. Soil Mech. Found. Div.* **97,** 1249–1273.
Seed, H. B., L. F. Tokimatsu, L. F. Harder, and R. M. Chung (1985). Influence of SPT procedures in soil liquefaction resistance evaluations, *J. Geotech. Eng.* **111,** no. 12, 1425–1445.
SigmaPlot software (2006). SigmaPlot for Window, version 10.0, http://sigmaplot.co.uk/products/sigmaplot/sigmaplot-details.php (last accessed February 2016).
Toprak, S., and T. L. Holzer (2003). Liquefaction potential index: Field assessment, *ASCE J. Geotech. Geoenviron. Eng.* **129,** no. 4, 315–322.
Weibull, W. (1951). A statistical distribution function of wide applicability, *J. Appl. Math.* **18,** no. 3, 293–296.
Wessel, P., and W. H. F. Smith (1991). Free software helps map and display data, *Eos Trans. AGU* **72,** 441.
Williams, R. A., J. K. Odum, W. J. Stephenson, and R B. Herrmann (2007). Shallow P- and S-wave velocities and site resonances in the St. Louis region, Missouri-Illinois, *Earthq. Spectra* **23,** 711–726.
Worden, C. B., and D. J. Wald (2016). ShakeMap manual online: technical manual, user's guide, and software guide, *U.S. Geol. Surv.*, doi: 10.1234/012345678.
Youd, T. L. (1973). Liquefaction, flow, and associated ground failure, *U.S. Geol. Surv. Circular 688*, http://pubs.er.usgs.gov/publication/cir688 (last accessed October 2016).
Youd, T. L., I. M. Idriss, R. D. Andrus, I. Arango, G. Castro, J. T. Christian, R. Dobry, W. D. L. Finn, L. F. Harder, M. E. Hynes, K. Ishihara, J. P. Koester, S. S. C. Liao, W. F. Marcuson, G. R. Martin, J. K. Mitchell, Y. Moriwaki, M. S. Power, P. K. Robertson, R. B. Seed, and K. H. Stokoe (2001). Liquefaction resistance of soils: Summary report from the 1996 NCEER and 1998 NCEER/NSF workshops on evaluation of liquefaction resistance of soils, *J. Geotech. Geoenviron. Eng.* **127,** no. 10, 817–833.

Chris H. Cramer
Kathleen Tucker
Center for Earthquake Research and Information
University of Memphis
Memphis, Tennessee 38152-3050 U.S.A.
ccramer@memphis.edu

Robert A. Bauer
Illinois State Geological Survey
Champlaign, Illinois 61820 U.S.A.

Jae-won Chung
J. David Rogers
David Hoffman
Missouri University of Science and Technology
Rolla, Missouri 65409 U.S.A.

Larry Pierce
Vicki Voigt
Brad Mitchell
David Gaunt
Missouri Geological Survey
Rolla, Missouri 65402 U.S.A.

Robert A. Williams
Oliver S. Boyd
Connor M. Watkins
Natasha S. McCallister
U.S. Geological Survey
Golden, Colorado 80401

Gregory L. Hempen
St. Louis, Missouri

Phyllis J. Steckel
Earthquake Insights LLC
Washington, Missouri 63090

Published Online 9 November 2016